Polymer Testing 131 (2024) 108326

Contents lists available at ScienceDirect

Polymer Testing

journal homepage: www.elsevier.com/locate/polytest

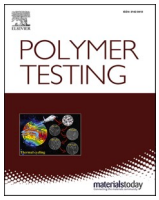

Comparison of the effect of thermal and hygrothermal sub-Tg aging on the durability and appearance of multilayered filament wound composite structure

Chaman Srivastava [a,**], Ben Alcock [b], Are Strandlie [a], Sotirios A. Grammatikos [a,*]

[a] ASEMlab – Laboratory for Advanced and Sustainable Engineering Materials Research, Department of Manufacturing and Civil Engineering, Norwegian University of Science and Technology, Gjøvik, 2815, Norway
[b] SINTEF Industry, Polymer and Composite Materials Group, Oslo, 0373, Norway

ARTICLE INFO

Keywords:
Polymer composite
Filament wound composite
Durability
Thermal aging
Hygrothermal aging

ABSTRACT

The study conducts an experimental investigation to compare the effect of accelerated aging on a glass fiber/vinylester matrix filament wound composite. Two static aging conditions, thermal and hygrothermal, were chosen. Samples were aged at temperatures below the glass transition temperature (Tg) of vinylester for 224 days. Mechanical test – ILSS and flexure testing and physicochemical assessments – DMA, FTIR and colorimetry were conducted to gauge the aging effects on long-term durability and appearance. Results are presented as retained property values over aging durations and environments. Notably, coupons aged below 60 °C under both conditions exhibited residual curing, enhancing mechanical properties. Time-temperature coupling influenced behavior, with higher temperatures and longer durations leading to degradation. Hygrothermal aging at 80 °C prompted earlier degradation than thermal aging, highlighting moisture's impact. DMA revealed interfacial degradation for hygrothermally aged coupons, verified by fractography. Conversely, damping factor analysis indicated residual curing for thermally aged coupons. Results were confirmed through color change and FTIR, showcasing evolving chemical patterns with aging.

1. Introduction

Filament winding is used extensively to manufacture tubular composite structures. The most common industrial uses of these Filament-Wound Composite structures (FWCs) are in the form of composite pipes for water and oil transport as marine risers and jumpers [1,2], grain silos in the farming industry [3], composite insulators in electrical equipment [4], etc. FWCs are most commonly made using filament winding of prepreg tapes or wet-winding, where resin-impregnated fiber filaments are wound around a plastic or metallic mandrel, making it different from traditional methods, which usually involve stacking followed by resin impregnation. The winding direction and tension affect the mechanical properties [5]. The winding angle and number of layers are selected based on the application. Hence, FWCs are characterized by high anisotropy at the macroscale [6]. Unique fiber reinforcements and matrix combinations can be chosen during the winding process to enhance corrosion resistance and structural integrity [7,8].

FWCs in civil engineering applications like oil and gas exploration are traditionally made of glass fiber-reinforced polymers (GFRPs). During their service life, these structures are often exposed to service environments like heat, humidity exposure, freeze-thaw cycles, etc. Manufacturing parameters like off-axis winding angles and tension have been found to cause premature micro-cracks and fiber-matrix interfacial degradation [9] when exposed to harsh environments. Hence, understanding the durability of FWCs is of utmost importance and can be assessed in laboratory settings using accelerated aging to determine the loss in structural integrity as a function of material degradation. The approaches to study degradation can be non-mechanistic [10] or mechanistic [11], where micro-structural changes like cracks, fiber-matrix interface degradation, etc., are accounted for. A better understanding of mechanisms behind the degradation is envisaged to allow for the prediction of expected lifetime [12]. The literature reporting the aging and durability of composites composed of glass fiber/vinyl ester matrix for civil engineering is abundant. However, there are few

* Corresponding author.
** Corresponding author.
E-mail addresses: chaman.srivastava@ntnu.no (C. Srivastava), grammatikos@outlook.com (S.A. Grammatikos).

https://doi.org/10.1016/j.polymertesting.2024.108326
Received 5 December 2023; Accepted 3 January 2024
Available online 4 January 2024

representative studies on the accelerated aging and long-term performance of FWCs with valuable data for designers. Very recently, to support designers in terms of specifications for the design of civil engineering structures, a recent technical specification has also been published [13] in an attempt to determine reduction factors based on the most corrosive environments and degradation mechanisms like (a) post curing (b) swelling/shrinkage coupled with micro-cracking, (c) plasticization (d) decomposition, etc., and by that create a framework to assess the degradation and approximate the service life or the residual properties over a specific timeframe.

The combined effects of temperature and moisture on the properties of FWCs are harsh over time. As aforementioned, when aging below glass transition temperature (Tg), glass fibers are very stable and not prone to degradation [14], but the matrix and fiber/matrix interface undergoes degradation that affects the mechanical and physicochemical properties of the composite over time. Physico-chemical analysis can help quantify microstructural changes like the degree of crosslinking, chain scission within the polymeric matrix, and fiber/matrix interface degradation as a function of aging temperature and duration. When a polymeric matrix is exposed to hygrothermal aging, the matrix's property changes occur along with moisture diffusion. This process follows Fickian absorption behavior under ambient exposure conditions. Plasticization of the matrix is observed in the early stages of hygrothermal aging and leads to a decrease in the Tg due to higher chain mobility [15]. As the temperature of aging, immersion time, or both are increased, polymer relaxation [16], residual crosslinking, and selective leaching of the low molecular weight polymer chains occurs [17], thus resulting in the removal of unbound and bound segments, which act as plasticizers as also reported by Zhou et al. [18]. This increases the glass transition temperature and diffusion kinetics, leading to a non-Fickian water absorption behavior.

In the case of thermal aging, when composites are aged in temperature ranges close to the Tg of the polymeric matrix, the degradation is primarily caused by softening, decomposition, and eventual mass loss [19] of the polymer, which is more prominent in an oxidizing environment as compared to vacuum or inert atmosphere [20,21]. Oxidation of the matrix is commonly reported at the beginning of the aging regime. Oxidation is superficial and is limited to the exposed surface until micro-cracks appear, leading to deeper diffusion of oxygen and bulk degradation, as reported by Pochiraju et al. [22] for multiaxial composites like FWCs. Long-term exposure to the thermal environment increases the composites' density and with slight shrinkage [23], contrary to hygrothermal aging environments where swelling is more commonly occurring.

The fiber/matrix interface and interphase region are also susceptible to damage and degradation when exposed to thermo-oxidative and hygrothermal environments like humidity and moisture. In the case of hygrothermal aging, prolonged exposure can lead to reversible, i.e., physical changes and irreversible which are chemical changes in the fiber/matrix interaction zone [15]. The diffusion of water leads to a reduced adhesion between the fiber/matrix interface, which leads to the dissipation of residual stresses [24] and interfacial debonding due to the differential swelling of fiber and matrix. Plasticization of the interphase region [25] and capillary action or 'wicking' are also responsible for degradation in the interface region, where wicking leads to more pronounced degradation than water diffusion through the matrix [26]. In the case of thermal aging, the effect of thermo-oxiation on the fiber/-matrix interphase was studied by Skourlis et al. [27] and a lower Tg was reported for the interphase region compared to the bulk of the resin through fiber-fragmentation tests. It was observed that faster degradation of the interphase region occurs at temperatures close to and above Tg of the resin. The difference in the thermal expansion coefficients of the fiber and matrix is also reported to cause micro-cracks in the matrix and at the fiber/matrix interface [28], which leads to failure. Another key issue with aging is an irreversible change in the texture and color of the composites. Combined effects of thermos-oxidation [20,29], moisture [30], and temperature [31] cause yellowing of resin and hence hinder the use of composite where aesthetics is crucial. In the case of exposure to water and elevated temperature, yellowing is observed due to the creation of carbonyl groups during chemical reactions like curing, hydrolysis, and oxidation of the matrix [32]. For vinylester matrix-based composite, the creation of conjugated double bond C═C [33] and new chromophores like quinone with conjugated groups [34] are reported to be the main cause behind yellowing.

This work aims to assess the long-term performance and appearance of FWCs under exposure to thermal and hygrothermal aging environments. Numerous studies have been presented in the literature for different combinations of fiber and polymer systems, but mainly in a single environment. Studies on glass fiber-vinylester based FWCs from an as-manufactured tubular structure comparing two prominent aging environment and their effects at sub-Tg aging temperature are scarce. Moreover, vinylester resin is corrosion-resistant; hence, the importance of physical and chemical degradation is highlighted at sub-Tg temperature within the allowable service environment. The test is carried out in the presence of the polymeric liner, hence also addressing degradation in a layered structure. The colorimetric analysis in the presence of a translucent liner could correlate with the in-service appearance changes on the surface of structures made from filament winding, which adds to the novelty. On top of this, current specifications [13] lack information related to filament wound structures used in civil engineering, and hence, this study can be a part of new FWCs guidelines, which is the topic of this work.

In addition, this research reports experimental findings of an extensive investigation regarding the effects of thermal and hygrothermal aging on FWCs coupons obtained from a glass fiber/vinylester tubular structure. The samples were extracted from the curved shell of the tubular structure and aged at room temperature (23 °C) and three elevated temperatures of 40 °C, 60 °C and 80 °C for a period of up to 224 d, in two different aging mediums: convective heat (thermal) and distilled water (hygrothermal static). The percentage retention values are reported as changes in mechanical property whereas physicochemical (Fourier Transformed Infrared Spectroscopy-FTIR), visco-elastic (Dynamic Mechanical Analysis- DMA), and color changes (colorimetric analysis) are reported as a function of the aging environment and duration of exposure. A correlation of mechanical properties is presented against the physicochemical changes to identify and differentiate degradation mechanisms caused by the effects of moisture and elevated temperatures.

2. Materials and method

2.1. Composite coupon Preparation

A glass fiber/vinylester tape made from E-glass fiber tapes with silane-based sizing infused with vinylester resin is used to produce the filament-wound composite structure using wet-filament winding. The tow is overwrapped over a liner. The overwrapping is carried out in the helical direction, followed by the hoop direction. After curing, the filament wound composites are stored at room temperature. An ATM Brilliant 220 precision wet abrasive cutting machine is used for cutting the coupons out of the filament-wound composite structure.

The test coupons are obtained along the axial direction (as shown in Fig. 1) of the composite structure with the liner attached to one side of the coupons. After cutting, the specimens were stored in sealed plastic bags at room temperature before aging.

2.2. Conditioning and accelerated aging for 224 days

2.2.1. Hygrothermal aging

Hygrothermal aging was conducted using Grant Sub Aqua Pro-unstirred water baths, with temperature stability of ±0.2 °C. Before being placed in heated water baths, coupons mass stabilized i.e., were

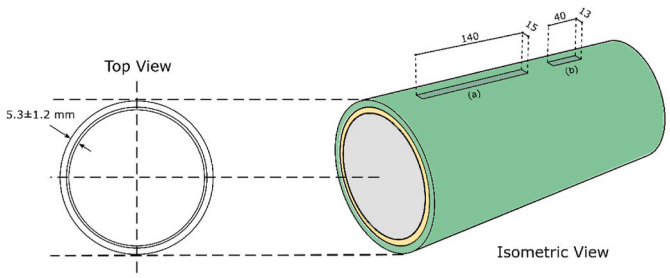

Fig. 1. Dimensions of filament wound structure with specimen extraction position, size, and direction (a) Flexure (b) SBS-ILSS coupon.

dried in a vacuum oven at 40 °C for 72 h to remove any potential moisture absorbed by the environment. The dried specimens were aged at 23 °C, 40 °C, 60 °C and 80 °C under complete immersion. Distilled water is used as a hygrostatic aging medium. The maximum aging temperature selected is below the Tg value of the unaged composite coupon. Coupons were removed from the water bath after each aging interval and kept in sealed bags in a refrigerator (4 °C) until testing, identical to storage conditions presented in Refs. [15,35–37].

2.2.2. Thermal aging

The composite coupons obtained from FWCs were placed in Termakrs oven with fan-controlled airflow to thermally age the coupons at temperatures of 23 °C, 40 °C, 60 °C and 80 °C in the presence of oxygen. The limiting temperature is selected to be lower than the Tg of the unaged coupon to avoid unwanted changes caused during the viscous transformation in the chemical structure of the polymer. The coupons were mass-stabilized identical to procedure used for hygrothermal aging i.e., excess moisture was removed before start of aging regime. To age at room temperature (23 °C), the coupons were kept in a box lined with silica gel desiccant to absorb moisture. Storage protocol identical to hygrothermal aging was used.

Before testing, the aged coupons were conditioned overnight to bring them to room temperature for both aging conditions. Hence, the storage and pre-test conditioning was kept the same for each batch of the coupons tested. A summary of test details is provided in Table 1.

2.3. Gravimetric analysis

The change in mass of the composite specimens during the water uptake test was measured according to ASTM D5229 [38]. Coupons were machined in dimensions of 100 × 100 × 5 mm. For water uptake measurements, coupons were removed from the water, and the surfaces were dried using a dry cloth and weighed in a micro-balance with an accuracy of 0.001 mg. The specimens were then placed back in the respective water baths. Four replicates were used in each aging temperature level. The weight change (%w) was calculated according to Equation (1).

$$w(\%) = \left(\frac{w_i - w_f}{w_i}\right) \times 100 \tag{1}$$

where w_i and w_f are the weights of the specimens from the water bath before and after water uptake intervals, respectively. The maximum water ingress attained at a specific temperature is calculated using the Fickian long-term diffusion model [39], which describes the moisture content inside the specimen at a specific period using Equation (2).

$$M_t = M_m\left[1 - \frac{8}{\pi^2}\exp\left(\frac{-Dt}{h^2}\pi^2\right)\right] \tag{2}$$

where M_t the percentage of the moisture gain and M_m is the maximum moisture concentration at a specific temperature. The data from the water uptake results at different temperatures are fitted to Eq. (2) using non-linear fitting and least square approximation method.

2.4. Mechanical testing – ILSS and flexural testing

Interlaminar shear strength (ILSS) testing using short beam shear composite coupons is most effective when using unidirectional laminate. However, this procedure has been used to assess the relative degradation in the matrix and, hence, the composite performance for non-unidirectional testing. Five coupons per aging type and duration were tested. The nominal dimensions of the coupons were selected according to the ASTM D2344 [40], and the tests were performed on an Instron 5966 universal testing machine with a maximum capacity of 10 kN. A span length of 22 mm was selected approximately four times the average thickness of the composite coupon. The roller diameter for the loading and support pin is 5 mm, and the loading rate is 1 mm/min. The interlaminar strength is calculated, where τ (MPa) is the apparent interlaminar shear strength, P_m (N) is the first failure load (a drop of 10 %) in the force-displacement curve, b (mm) is the average width and h (mm) is the average thickness of the short beam shear coupon. The interlaminar shear strength was calculated using Eq. (3).

$$\tau = 0.75\frac{P_m}{bh} \tag{3}$$

Flexural testing allows qualitatively assessing the matrix and the fiber matrix interfacial strength degradation. Coupon dimensions were selected according to ASTM D7264 [41] for the three-point flexural testing. The flexure stress and strain were presented in Eq. (4).

$$\sigma = \frac{3PL}{2bh^2}$$
$$\varepsilon = \frac{6\delta h}{L^2} \tag{4}$$

where, P is the force (kN), L (mm) is the span length, and δ is the mid-span deflection. Five coupons per aging type and duration were tested. The roller separation for the support pin was set to 80 mm with a span-to-thickness ratio of 16:1. The loading rate was set to 1 mm/min. The mechanical testing was carried out at regulated lab temperature, where the average temperature is ±24 °C.

2.5. Measurement of color change

A dedicated color change analysis was carried out to measure the color change and, hence, the coupons' appearance as a function of aging. The spectral radiance was measured between 380 and 780 nm using a D50 illuminant and CS2000 tele-spectroradiometer (TSR, Konica

Table 1
Nomenclature, parameters, aging environments, and the aging duration for determining mechanical property retention.

#	Service Environment	Aging Conditions	Type of Test	Temp (°C)	Duration (days)	Coupons
1	Thermal	Convective heat	Short beam shear (SBS), Flexure, DMA	Room temperature (23), 40, 60, 80	0, 28, 56, 112, 224	Temp(4)*Time(4)*TestType(3)*Rep(5) + Unaged(5) = 245
2	Hygrothermal	Immersion distilled water, unstirred Total = 506	Short beam shear (SBS), Flexure, DMA	Room temperature (23), 40, 60, 80	0, 28, 56, 112, 224	Temp(4)*Time(4)*TestType(3)*Rep(5) + Unaged(5) + Water Uptake (16) = 261

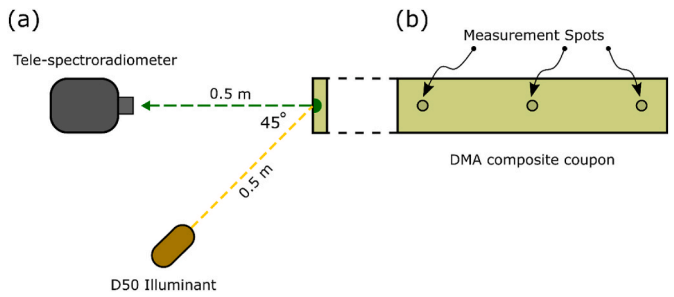

Fig. 2. (a-b) A schematic illustration for quantifying color measurements using a tele-spectroradiometer. (b) Measurement *spot size* = 5 mm.

Minolta), angled at 45° inclination. The optical resolution and the sampling interval of the scan were set to 1 nm. Data sampling was carried out at three positions at the sample's top, middle, and bottom, as presented in Fig. 2, and averaged over four repetitions. DMA coupons (presented in the following section) were employed for color analysis. The measuring device was calibrated using a standard spectral tile, and the measured radiance was averaged over three scans at one spot. To calculate the tristimulus colorimetric values (CIEXYZ), color engineering equations reported by Green et al. [42] were implemented in MATLAB r2020b. Color matching functions and weights were used per ISO 13655:2017 for a D50 illuminant.

The yellowing index (Y.I.) was calculated using ASTM E313-05 [43] where

$$YI = \frac{100(1.28x - 1.06z)}{y} \tag{6}$$

and x,y, and z are the measured tristimulus values of the sample after a specified aging environment, duration, and temperature. The overall change is measured as $\delta YI = YI^{env}_{T,t} - YI_o$ where $YI^{env}_{T,t}$ is the measured yellowing indices after aging and YI_o is the unaged reference.

2.6. Viscoelastic and physicochemical characterization - DMA and FTIR

Viscoelastic and physicochemical characterization of the FWC coupons was carried out using Dynamic Mechanical Analysis (DMA) and Fourier Transform Infrared Spectroscopy (FTIR) to identify changes in the composite (predominantly the vinyl ester matrix) as the aging process progresses. To identify changes in the visco-elastic properties of the bulk composite material, changes in the Tg (calculated from the peak value of the Tan δ curve) were monitored for both thermally and hygrothermally aged coupons. A Discovery 850 by T A. Instruments (Delaware, USA) was employed for 3-point bending mode testing at a temperature range between 30 °C and 140 °C. The temperature range was kept constant for all coupons in this study.

Concerning FTIR, resin crumbs were scraped from the coupons' surface to study the material's chemical signature under an FTIR –ATR prism from Agilent Systems (Cary 630 FTIR, Santa Clara, USA). FTIR signals were recorded in the wavelength range of 400–4000 cm^{-1} at a scan speed of 3 scans/sec, while the signal was averaged over 24 scans. The peak height was calculated using Agilent Resolutions Pro software. A baseline correction and data normalization are done using the maximum peak height. For the calculation of the carbonyl index, the peak height was measured perpendicular to the baseline, joining two wave numbers for all FTIR spectra from different aging environments and durations.

3. Results and discussion

3.1. Gravimetric analysis- water sorption behavior

Fig. 3 presents the normalized changes in mass due to water uptake and the fitted 1D-Fickian of FWC coupons with the liner subjected to

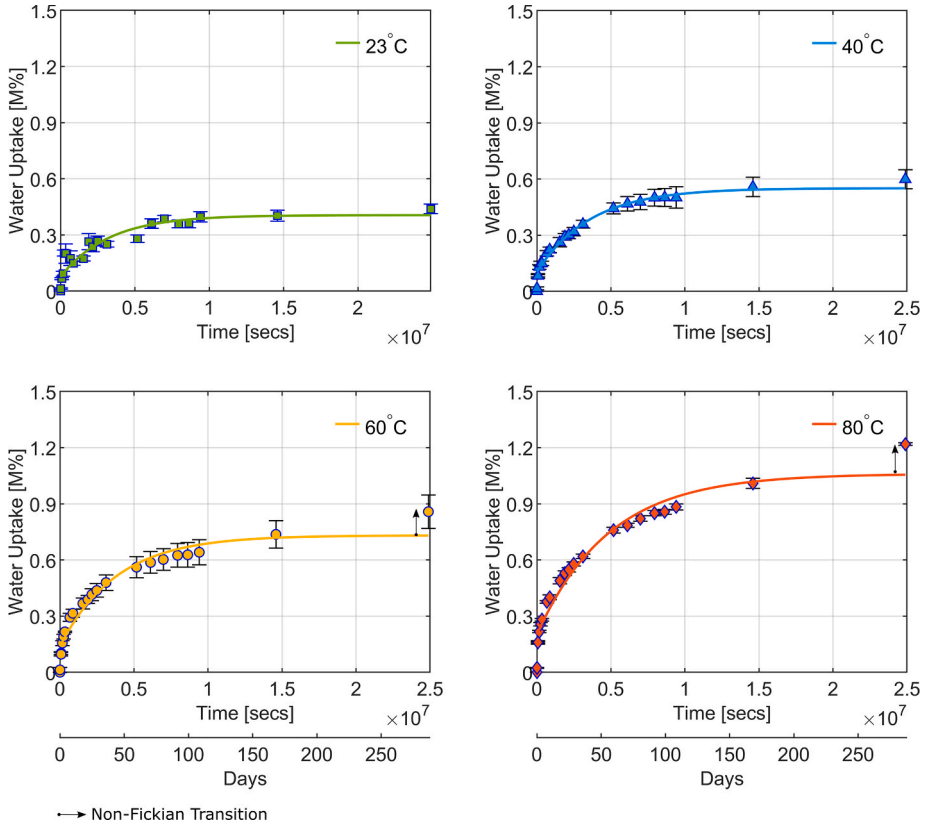

Fig. 3. Water uptake (w%) and fitted Fickian curves for hygrothermal aging at 23 °C, 40 °C, 60 °C, and 80 °C.

Table 2
Maximum moisture content values calculated by long-term 1D-Fick's law.

Temperature (°C)	M_m(%)
23	0.428
40	0.551
60	0.731
80	1.060

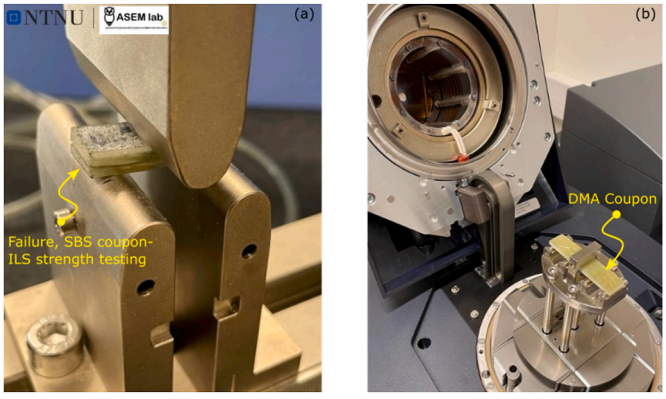

Fig. 4. (a) Universal Mechanical testing setup for ILSS testing showing failure in FWC coupon (b) DMA 3-point bending setup.

hygrothermal aging. The change in mass (w%) is plotted as a function of the exposure duration (secs/days) at aging temperature levels of 23 °C, 40 °C, 60 °C, and 80 °C in distilled water—the analysis aimed to identify the maximum water content as a function of temperature and immersion duration. The presence of liner would eventually not change the maximum water uptake but would prolong the time to achieve it. The water uptake behavior is roughly approximated as a Fickian response using the equations presented in Section 2.3 for all hygrothermal aging temperatures. The water uptake is significantly faster during the initial days of exposure due to higher diffusion kinetics and is observed as a linear region in the Fickian response. During prolonged exposure, a transition to a relatively flat curve is observed, which signifies reduced diffusion kinetics, and the coupons achieve water saturation. The maximum water uptake M_m signifying this saturation is measured respectively.

Table 2 presents the maximum moisture content as a function of immersion temperature. After long-term exposure (≈170 d), a transition to non-Fickian behavior was observed, revealing deviations in the moisture uptake curve to non-Fickian behavior. These deviations can be attributed to an interplay between physical and chemical changes that may occur inside the composite after prolonged exposure. Physical changes like the coalescence of voids and swelling effects due to water diffusion can lead to internal restructuring of the microstructure, causing more surfaces to be exposed and, hence, an apparent increase in the water absorption kinetics. Chemical changes like polymer relaxation [44,45], creation of free volume, and polymer network rearrangement leading to macro-molecule chain rearrangement are also responsible for an apparent increase in the moisture uptake values [46].

The maximum water uptake value was also 1.06 % for aging at 80 °C compared to 0.42 % for aging at room temperature, which agrees with literature findings for vinyl ester composites [47–49]. It can also be postulated that water uptake in polymeric composites is dominated mainly by the matrix and the fiber-matrix interface, where the water uptake is dependent on the molecular structure, the polarity, and the degree of additional crosslinking at the time of exposure.

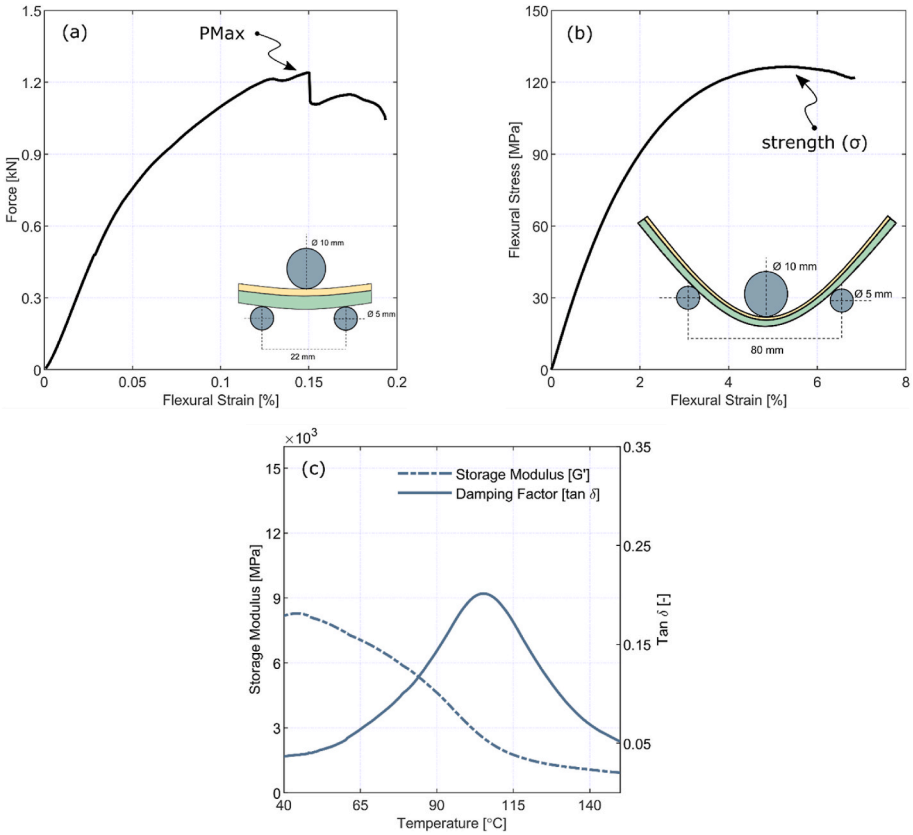

Fig. 5. Representative experimental curves of (a) ILSS testing, (b) flexural testing (c) DMA testing. Yellow is the liner, and green is the unaged FWCs composite layers.

3.2. Unaged coupons - reference

This section summarizes the results from the mechanical and physicochemical characterization of reference and aged composite coupons after thermal and hygrothermal aging. Fig. 4 presents the experimental setup for measurement of ILS strength using SBS composite coupons and DMA setup. Fig. 5 presents representative experimental curves for (a) ILSS testing, (b) flexural testing, and (c) dynamic mechanical analysis. The behavior of the stress-strain curves for both (a) and (b) is linear at the beginning, followed by a non-linear region until failure. For ILSS testing, the maximum force before the failure is taken as the P_{max} point for the onset of delamination. The failure is observed as splitting the laminates at one of the ends of the specimen. In contrast, during flexural testing, there is no apparent instantaneous failure observed; therefore, the point at which the stress-strain curve starts to drop was taken as the ultimate flexural strength (σ_f).

Fig. 5(c) presents the unaged composite coupon's storage (dashed line, G′) and tangent modulus. The response of the unaged composite for the tangent modulus (tan δ) is a typical sigmoidal curve, which is very common in polymeric-reinforced composites. To quantify the effect of aging on Tg, the horizontal shift of $(\tan\delta)$ peak is used to compare the change in Tg and any potentially related crosslinking, plasticization, etc. A vertical shift was used to characterize degradation in the interface of the fiber and matrix and damping due to residual crosslinking during the aging [50]. A summary of mechanical and physico-chemical properties of unaged FWC coupons is provided in Table 3.

The recorded FTIR spectra were similar to typical vinyl ester polymers, with significant indexed peaks from functional groups presented in Table 4. The signal from the unaged coupons peak at 1722 cm^{-1} can be observed, which could be from the ester and the adipate groups, a common plasticizer for vinyl ester-based composites. The extent of degradation and degree of yellowing can also be assessed by calculating the changes in peak height as a function of the aging temperature and time. A weak polystyrene peak (697 cm^{-1}) is also observed, a typical polymerization product of styrene solvent during the curing of glass fiber vinylester composites. A hydroxyl peak can also be observed at 3310 cm^{-1}.

Table 3
Mechanical and physico-chemical properties of the unaged filament wound composite coupons.

Property	Method	Notation [Unit]	Reference Specimen
Mechanical Property	Interlaminar shear (ASTM D2344M − 13)	σ_{obs} [MPa]	19.21 ± 2.12
	Flexural Testing (ASTM D7264M)	σ_f [MPa]	119.15 ± 16.71
		ε_f [%]	5.63 ± 0.54
		E [GPa]	5.39 ± 0.65
Glass Transition Temperature	DSC (ASTM D3418-21)	T_g [°C]	97.8 ± 5.8
	DMA (ASTM D7028-07)	T_g [°C]	105.1 ± 1.6
		T_g Onset [°C]	83.5 ± 3.3
Chemical Composition	FTIR	The absorbance spectrum matches closely with typical vinyl ester with bisphenol-A.	
Glass Fiber Content	Micro CT	(volume fraction %)	70 ± 3.3
	Calcination	(weight %)	68.2 ± 1.2

Table 4
FTIR spectra indexed peak data with functional groups from scans of polymer powder from composite.

Peak [Unit]	Range [cm^{-1}]	Functional Group	Property Correlation
1	3600–3200	–OH	Hydrolysis
2	2960–2850	$–CH_2$, –CH, $–CH_3$	Used a peak reference
3	1725–1705	–C═O	Degradation/Yellowing
4, 5	1600–1500	–C═C, Quinone	Yellowing

3.3. Mechanical characterization

3.3.1. Effect of aging on interlaminar shear response

The measure of interlaminar shear strength as a function of aging time and temperature can provide an insight into the degradation of the matrix between the reinforcing laminates of the composite. Interlaminar shear stress evolution vs. the midspan deflection for composite coupons for each aging interval, is calculated using the relevant standard. As is illustrated by Fig. 5(a), for ILSS, the force displacement relationship is initially linear (elastic) but then softens and becomes non-linear (plastic). This behavior could be attributed to the multilayered (liner and FWC) structure of the material under investigation, both contributing to the loading response. The failure in SBS coupon is observed as a sharp drop in the force-displacement curve with a crack opening in the FWC composite layer as shown in Fig. 4 (a) and correlated to force-displacement curve in Fig. 5 (a). It is worth noting that no separation between the FWC composite layer and liner was obtained during ILSS testing, for all tests performed. The point of the first failure was considered as a point where the force-displacement curve falls more than 15 % of the peak force value. This force value is considered the maximum load for the calculation of the ILS strength values. The ILSS retention values were calculated (P_{max}) and averaged for 5 specimens per each aging interval for the individual aging regimes [15]. It was observed from the ILSS behavior of the material exhibits a time-temperature coupling for both the thermal and hygrothermal aging regimes, while 3-transition stages were identified. During the initial days of aging, a "consolidation phase" was visible, with an increase in properties P(t), followed by a "reduction phase", attributed to the decrease in properties from the "consolidation phase" but P(t) > 100 %. A "degradation phase" is also observed where the properties for aged coupons were below the unaged case i.e. P(t) < 100 %. For reasons of simplicity, the effects of aging can be categorized into short- and long-term aging effects where the former addresses the time frame between 0 and 56 d, and latter for aging between 56 and 224 d. The transition of 56 d was purposely chosen as the point after which the properties exhibit a significant change. To assess the durability of the composite structure at temperatures below the glass transition temperatures, it has been observed that the durability properties are mostly dominated by the resin [51].

Fig. 6 (a–d) presents the ILSS retention values of FWC hygrothermally aged coupons, as a function of aging duration (days). After 56 d of accelerated aging, ILSS values increase for all aging temperature levels except 0.75 Tg (80 °C), while the maximum strengthening effect is visible for aging at 60 °C after 112 d. This strengthening effect can be attributed to additional crosslinking of vinyl-ester at temperatures well below Tg, and hence the interlaminar shear strength, which is a matrix-dominated property, increases [46]. This strengthening effect seems to depend on the synergistic effect of the temperature and duration of aging, which is 'masked' by significant degradation for the case of aging at 80 °C, where in the interplay between degradation and post curing. It

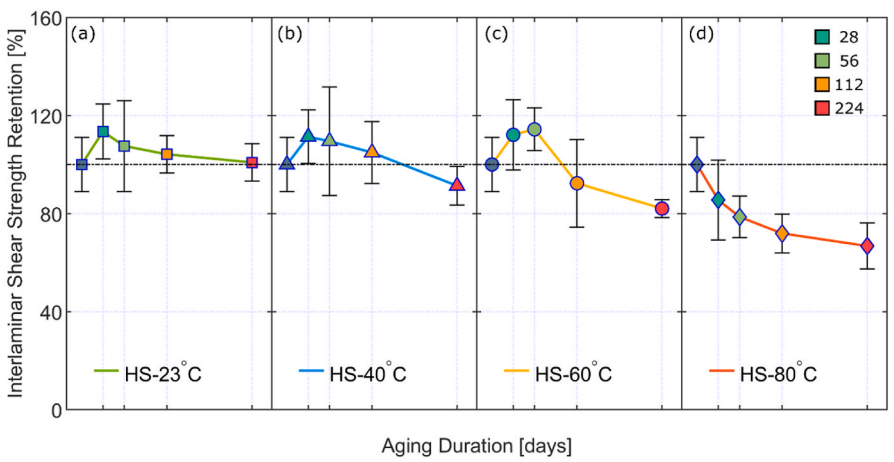

Fig. 6. Average ILSS retention values of the hygrothermally aged FWCs at 23 °C, 40 °C, 60 °C and 80 °C.

can be hypothesized that the residual strengthening during the "consolidation phase" during the initial days of exposure subdues any ongoing degradation, resulting into an increase in ILSS values.

For longer term effects, a "reduction phase" follows after the "consolidation phase", for the cases of aging at 23 °C, 40 °C and 60 °C. After the initial ILSS values increase, the "reduction phase" illustrates ILSS values decrease, to lower levels of ILSS than the original case (unaged/100 %), apart from the case of aging at 23 °C, for which as aforementioned ILSS values practically return to the initial stage [52]. This anomalous behavior at low temperatures, can be attributed to secondary bonding of the polymeric and water molecules at lower temperature [18]. The degradation can be attributed to the plasticization of the matrix [18,53] and differential swelling between the fiber and matrix [25]. Hydrolytic leaching of the silane sizing on the fiber/-matrix interface has also been reported to cause eventual degradation within the laminate, which can be visible as swollen pitted regions on the fiber surface and which can eventually lead to fiber failure [52,54]. Similar observation was observed during the fractographic analysis as well, presented in Section 3.4.

After aging for 224 d, it was revealed that the maximum reductions of 8.7 %, 17.96 % and 33.24 % were observed for aging at 40 °C, 60 °C and 80 °C, respectively (no aging was observed for the case of aging at 23 °C). Hence it can be concluded that accelerated aging at relatively low temperatures (23–40 °C), does not lead to significant degradation in the time periods investigated in this work. Table 5 presents all calculated mean ILSS values and their corresponding standard deviations, of the material subjected to hygrothermal aging.

Fig. 7 (a–d) presents the ILSS values of the thermally aged FWC coupons. The general trend of ILSS values, for the case of thermal aging, varies again for both the aging duration and temperature. For short term aging effects, the ILSS values for all aging regimes increase, and is observed as a "consolidation phase". This strengthening effect can be attributed to additional crosslinking of vinyl ester, and, hence, the interlaminar shear strength (which is a matrix dominated property) increases. The initial strengthening is often due to time temperature coupling, where higher temperature causes higher increase in the matrix dominated properties for vinylester based composites [55].

For longer-term aging effects (56, 112 and 224 d), ILSS values drop, with the aging at 80 °C inducing the most significant degradation in ILSS, as aging temperature gets closer to the unaged FWC Tg. For lower temperatures (23 °C and 40 °C, $T < 0.5$ Tg), ILSS values plateau, towards the end of aging duration. The final values are above 100 %, or in other words degradation is absent. To understand this behavior where the P(t) plateaus, it can be hypothesized that the presence of the micro-cracks during the aging may help to create crevices where the oxygen can percolate. This effect can create an oxide layer and thus aids in the oxidation of the whole polymer. In the case of fiber composites from filament wound composites, it is observed that due to the presence of fibers in the hoop layer which is parallel to the surface of the composite, the oxide layer is arrested and hence the diffusion of the oxygen is arrested, which protects the bulk of the coupon to remain unaffected [56]. A degradation phase is observed at 80 °C with a reduction of 17.74

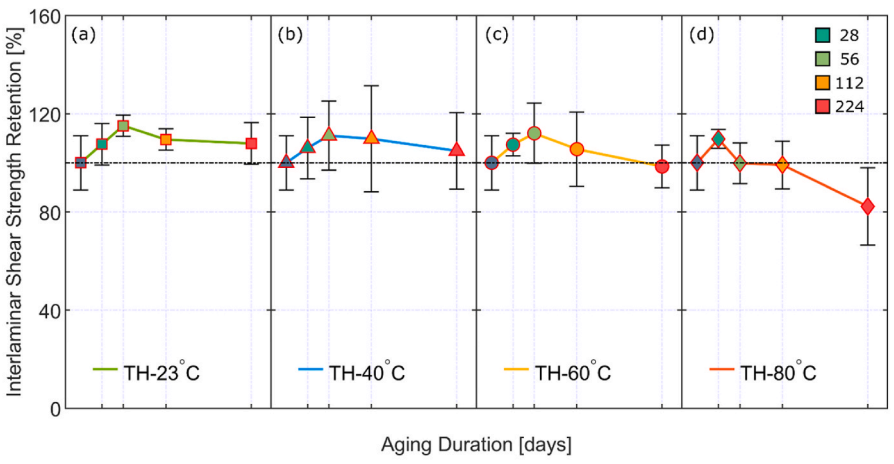

Fig. 7. Average ILSS retention values of the thermally aged FWCs at 23 °C, 40 °C, 60 °C and 80 °C.

Table 5
Average ILSS percentage retention values and corresponding standard deviation for hygrothermally aged FWC coupons.

Days	Room Temperature (23 °C)	40 °C	60 °C	80 °C
(%)				
28	113.44 ± 11.24	111.32 ± 10.90	112.10 ± 14.31	85.49 ± 16.33
56	107.53 ± 18.54	109.49 ± 22.14	114.33 ± 8.72	78.65 ± 8.44
112	104.15 ± 7.61	104.88 ± 12.60	92.36 ± 17.86	71.90 ± 7.92
224	100.85 ± 7.60	91.30 ± 7.85	82.04 ± 3.68	66.76 ± 9.35

Table 6
Average ILSS percentage retention values and corresponding standard deviation values for thermally aged FWC coupons.

Days	Room Temperature (23 °C)	40 °C	60 °C	80 °C
(%)				
28	107.57 ± 8.51	106.04 ± 12.53	107.39 ± 4.58	110.34 ± 3.85
56	115.13 ± 4.31	111.11 ± 14.11	112.04 ± 12.27	99.85 ± 8.28
112	109.48 ± 4.35	109.79 ± 21.60	105.57 ± 15.15	99.17 ± 9.72
224	107.90 ± 8.46	104.86 ± 15.58	98.52 ± 8.76	82.26 ± 15.74

% at the end of 224 d. Table 6 tabulates all ILSS values for thermally aged FWC coupons. Comparing Tables 5 and 6, one can conclude that the combined effects of water and temperature are more detrimental to matrix dominated properties like ILSS when compared to pure thermal exposure. A degradation contourmap comparing the effects from the study is presented in Ref. [57].

3.3.2. *Effect of aging on flexure response*

Effects of hygrothermal and thermal aging on flexural properties of the studied FWC material is presented in this section. Flexural modulus (E), flexural strength (σ_u) and their retention as a function of aging time and temperature is discussed. As can be seen by Fig. 5(b) the failure in the composite coupons is similar; a transverse crack through the composite thickness leads to a drop in the load-displacement curve. Figs. 8 and 9 and Table 7 and 8 illustrates and present the percentage retention (%) values of flexural stiffness for hygrothermally and thermally aged coupons, respectively, at the aging temperature of 23 °C, 40 °C, 60 °C and 80 °C.

In the case of flexure stiffness for both the hygrothermal and thermally aged FWC coupons, an irregular non-monotonic behavior was recorded, with signs of property recovery at lower temperature towards the end of aging regime. In the case of short term hygrothermal aging, no "consolidation phase" was visible at 23 °C but a high strengthening effect can be seen for aging at 40 °C, that is followed by a reduction phase. Reversal in the properties is observed for aging at 60 °C, wherein the

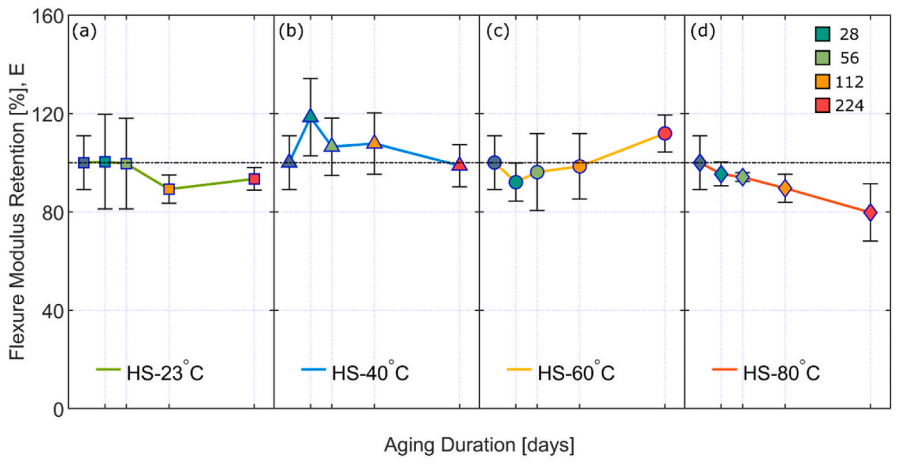

Fig. 8. Average flexural modulus retention values as a function of time for hygrothermally aged FWC coupons.

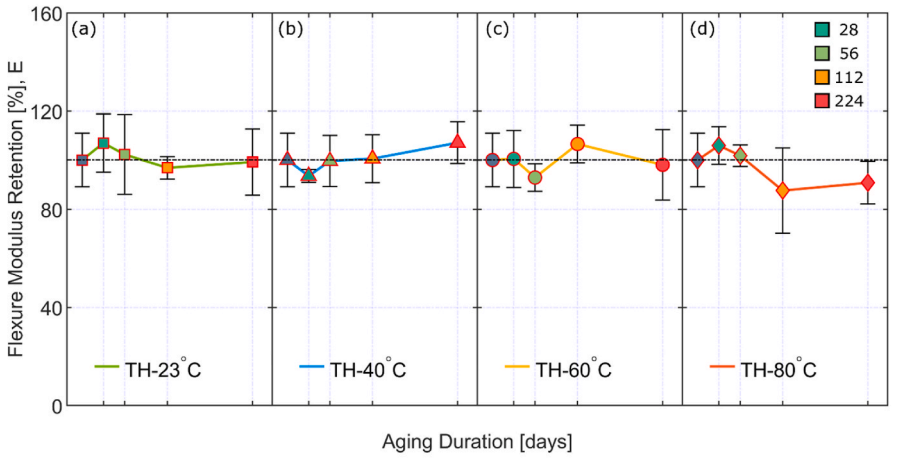

Fig. 9. Average flexural modulus retention values as a function of time for thermally aged FWC coupons.

Table 7
Average flexural stiffness of hygrothermally aged FWC coupons and corresponding standard deviation.

Days	Room Temperature (23 °C)	40 °C	60 °C	80 °C
(%)				
28	100.32 ± 19.21	118.44 ± 15.70	92.05 ± 7.76	95.32 ± 4.82
56	99.58 ± 18.39	106.45 ± 11.64	96.12 ± 15.63	94.12 ± 1.78
112	89.20 ± 5.70	107.72 ± 12.43	98.46 ± 13.32	89.57 ± 5.71
224	93.39 ± 4.59	98.75 ± 8.55	111.84 ± 7.45	79.70 ± 11.65

Table 8
Average flexural stiffness of thermally aged FWC coupons and corresponding standard deviation.

Days	Room Temperature (23 °C)	40 °C	60 °C	80 °C
(%)				
28	106.95 ± 11.88	93.52 ± 2.59	100.47 ± 11.59	105.92 ± 7.73
56	102.25 ± 16.22	99.62 ± 10.47	92.89 ± 8.64	101.79 ± 4.42
112	96.83 ± 4.54	100.56 ± 9.74	106.53 ± 7.73	87.57 ± 17.42
224	99.16 ± 13.50	107.05 ± 8.44	98.04 ± 14.31	90.77 ± 8.67

properties improve overtime, after the initial stiffness loss after 56 d of aging. This strengthening can be attributed to residual post-curing and plasticization which activates at higher temperature also reported by Ref. [46]. A monotonic "degradation phase" of flexural stiffness was recorded for hygrothermal aging at 80 °C.

An interplay between moisture induced resin plasticization [58] and post-curing [15] which after a prolonged exposure can lead to degradation of fiber matrix interfacial debonding, matrix micro-cracking and hydrolytic leaching [59] could be hypothesized for degradation at higher temperatures.

In the case of thermal aging, it can be observed that overall the flexural stiffness degraded marginally, while a recovery in properties was recorded for aging temperatures 40 °C, 60 °C and 80 °C, after 56 d of aging. Although, as can be seen the calculated standard deviation of mean flexural stiffness values is high, which can be attributed to the different internal geometry of the test specimens. As has been reported, thermal aging below Tg of the matrix, is mostly dominated by matrix failure under the compression zone and fiber-matrix interfacial degradation. A non-monotonic behavior in flexural stiffness as an effect of isothermal aging was observed, for all studied aging temperatures, except for 40 °C, for which a slight increase in the flexural stiffness was recorded at the end of aging term.

Figs. 10 and 11 and Tables 9 and 10 illustrates and presents, flexural

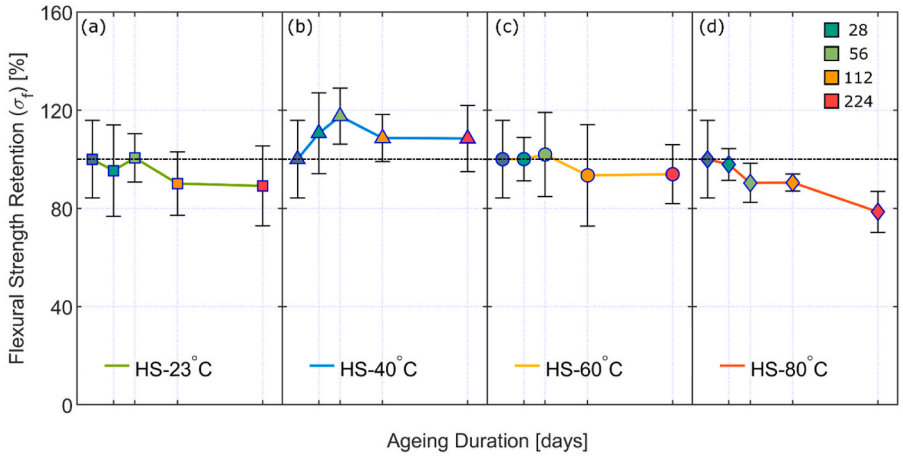

Fig. 10. Average flexural strength retention values as function of time for hygrothermally aged FWC coupons.

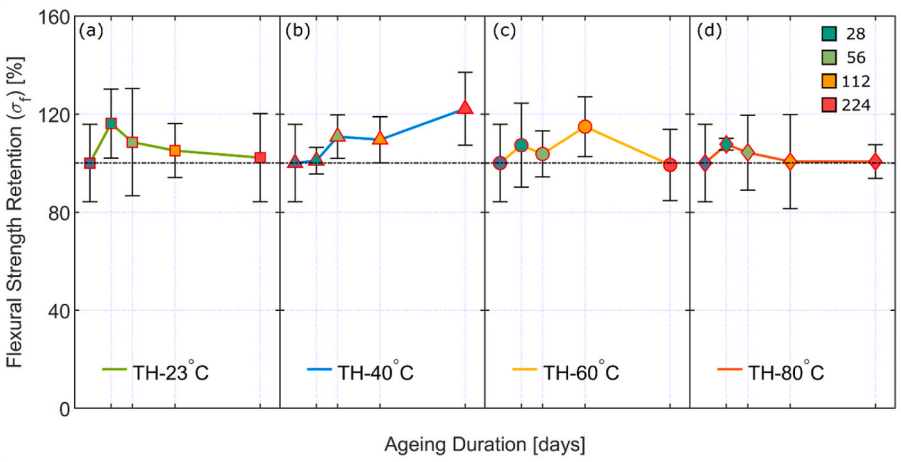

Fig. 11. Average flexural strength retention values as function of time for thermally aged FWC coupons.

Table 9
Average flexural strength values of hygrothermally aged FWC coupons and corresponding standard deviation.

Days	Room Temperature (23 °C)	40 °C	60 °C	80 °C
(%)				
28	95.33 ± 18.59	106.90 ± 16.47	100.05 ± 8.85	97.58 ± 6.45
56	100.58 ± 9.86	117.52 ± 11.41	101.92 ± 17.15	92.12 ± 7.99
112	96.41 ± 3.07	108.61 ± 9.57	106.40 ± 18.05	90.48 ± 3.44
224	98.63 ± 12.66	108.44 ± 13.49	93.90 ± 11.97	78.56 ± 8.38

Table 10
Average flexural strength values of thermally aged FWC coupons and corresponding standard deviation.

Days	Room Temperature (23 °C)	40 °C	60 °C	80 °C
(%)				
28	120.46 ± 11.80	100.96 ± 5.40	101.08 ± 11.63	106.81 ± 1.65
56	114.92 ± 19.15	107.76 ± 6.69	105.84 ± 9.31	110.33 ± 8.39
112	108.88 ± 8.10	112.78 ± 7.06	114.84 ± 12.21	105.58 ± 17.90
224	108.79 ± 11.83	122.17 ± 14.90	99.22 ± 14.54	100.56 ± 6.90

strength retention values for the hygrothermally and thermally aged FWC coupons, respectively. In the case of hygrothermal aging, in general, for both short and long term aging, a strengthening effect was observed followed by degradation. At 23 °C, it is observed that hygrothermal aging causes reduction in the mean values of strength, after 112 d and 224 d of aging, however, due to the increased scattering of the values, it cannot be postulated with confidence whether degradation is significant. For aging at 40 °C and 60 °C, a consolidation phase is observed followed by degradation for the latter. For aging at 80 °C monotonic strength loss was recorded. Being matrix dominated, flexural strength response is in close agreement with observations from ILSS testing.

In the case of thermal aging, as can be seen from Fig. 11, the flexural strength values exhibit a non-monotonic behavior, with a consolidation phase observed for all aging temperatures, followed by degradation (apart from the case of aging at 40 °C). At lower aging temperatures, strengthening is observed for aging at 23 °C after 28 d, which is followed by lowering in strength to values higher than the reference value (unaged). For the case of aging at 40 °C, strengthening is observed at the very early stage of aging, and continues until the end of term (224 d). As the aging temperature increases, the onset of degradation starts earlier which is observed at 112 d for 60 °C and 56 d at 80 °C. Thus a time-temperature dependency is observed which leads to higher post-curing effects at temperatures well below 0.5 Tg [20]. It can be hypothesized that pure thermo-oxidative aging in the presence of isothermal conditions leads to embrittlement of the matrix and hence micro-cracks which occur on the surface can lead to coupon failure.

3.4. Fractographic analysis

Fractography of composites is a complementary study to understand the failure behavior due to changes in the polymeric matrix, fiber, and the fiber/matrix interface. In this work, a crack opening was visible in SBS (Short Beam Shear) ILSS composite coupon, and the fractured surface of these coupons was used to study the changes in the morphology of the fiber and matrix as a function of aging temperature and duration of exposure. The failure in SBS coupons is mainly dominated by a mixed mode shearing [60,61], and hence the failure in a thermosetting polymer like vinyl-ester is dominated by river-mark lines, and micro-cracks which tends to generate delamination under an applied load, which leads to an eventual failure. To compare the effects of hygrothermal and thermal aging, two most aggressive environments and duration is selected viz: 80 °C at 224 d.

Fig. 12 presents the representative fractographic aspects observed in the SBS coupon fractured coupon surfaces aged in hygrothermal environments. The most common failure characteristics are (1) shear cusps, (2) pitted fiber surfaces and (3) river-marks and feathered appearances. The shear cusps in the matrix are identified as an inclined platelets at the edges and between the fibers. During the ILS strength testing, high shear at fiber/matrix interface causes cleavage of matrix and leads to cusps and river marks where the direction of steps created indicates the direction of the failure propagation [62]. Pit formation on fiber sizing was observed as well which could be potentially responsible for degradation of fiber/matrix interface [54]. Fiber/matrix debonding is also visible due to potential matrix dissolution and degradation of fiber/matrix interface.

Fig. 13 presents the representative fractographic aspects observed in the SBS coupon fractured coupon surfaces aged in thermal environment. It was observed that the matrix shows a predominant brittle failure with faceted cusps and scarps observed in the matrix tramlines between the

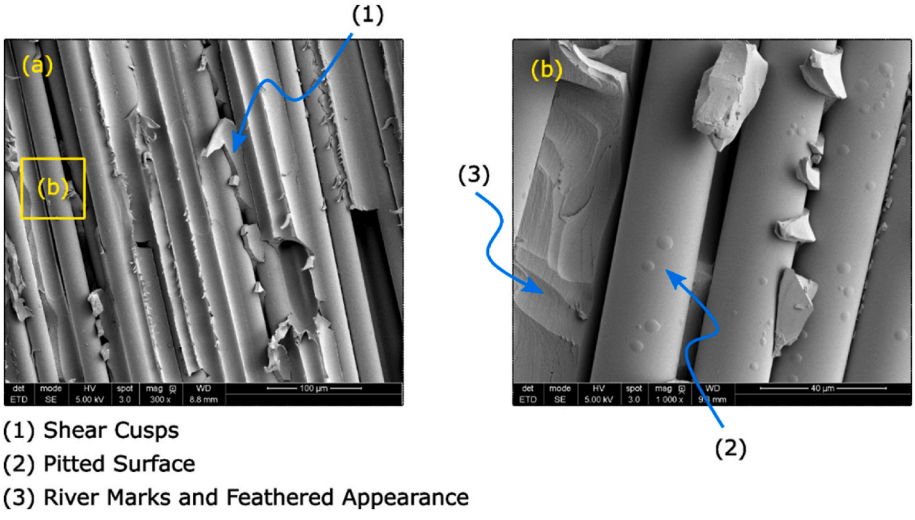

Fig. 12. Fractographic analysis of hygrothermally aged composite coupon failure surface aged at 80 °C at 224 days.(a) failure surface, fiber-matrix (b) zoomed inset.

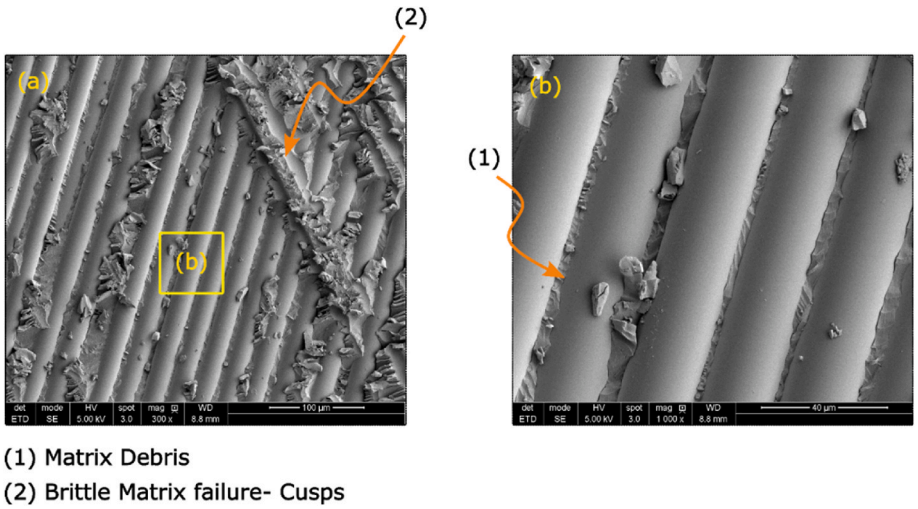

Fig. 13. Fractographic analysis of thermal aged composite coupon failure surface aged at 80C at 224 days: (a) failure surface, fiber-matrix (b) zoomed inset.

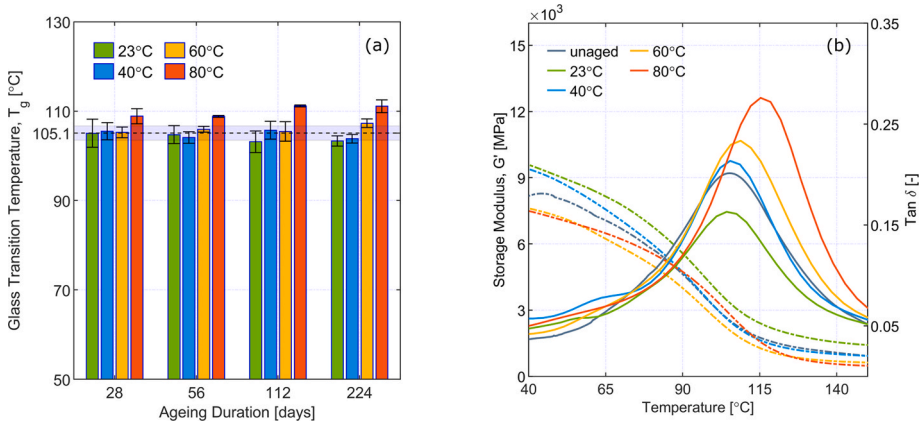

Fig. 14. (a) Variation of Tg values for hygrothermally aged FWC coupons for 28, 56, 112 and 224 days of exposure and (b) representative curves of tan δ and storage modulus as a function of aging temperature for 224 days of exposure.

fibers. This situation could be imagined where matrix behaves like a miniature tensile test and causes failure under an applied shear loading leading to serrated cusps as shown with marking (2). During failure, polymeric debris scattered all over the coupon surface. No fiber/matrix debonding and pitting of the fiber was observed during the investigation.

3.5. Viscoelastic and physico-chemical characterization

3.5.1. Dynamic mechanical analysis of aged composite coupon

The measure of the glass transition temperature, (Tg) of a polymeric composite material provides an insight into the relaxation behavior and its viscoelastic response. During testing, for temperatures below Tg, stiffness is typically unaffected. Above the Tg, the material softens due to an increase in the polymer chain mobility, which increases the flexibility and hence reduces the overall mechanical integrity of the polymeric composite structure. During service, composites are subjected to complex environmental conditions and hence a broad overview and correlation of changes in the Tg, under different aging environments becomes critical.

Fig. 14 (a) presents the changes in Tg values as a function of aging in hygrothermal environments at 23 °C, 40 °C, 60 °C and 80 °C respectively and (b) representative DMA curves at 224 d of aging at different aging temperature. As can be seen, the changes follow a slight time-temperature coupling, presenting a higher increase in Tg at higher temperature and longer duration of aging. In the case of short-term aging, Tg values remain unaffected for lower temperature hygrothermal aging (below 0.5 Tg, 23 °C, 40 °C and 60 °C) and is well within the standard deviation (blue shaded area) of the unaged specimens. An apparent increase in Tg values is recorded for aging at 80 °C where the Tg increase nearly by 3.7 °C. For long-term aging, and low aging temperatures, the changes in Tg values are minimal where an apparent change of −1.8 °C, −1.3 °C and 2.2 °C is observed for aging at 23 °C, 40 °C and 60 °C after 224 d of aging. The changes with the standard deviations are negligible and can be taken as "unchaged" as a function of aging time and temperature. Substantial changes in Tg values were obtained for aging closer to the Tg values of the unaged material. At 80 °C, the Tg values increase with an increment of 6.3 °C was observed after 224 d of exposure. It can also be noted that the visco-elastic response i.e. the peak of the damping factor increases as the temperature of the aging is increased shown exemplary in Fig. 14 (b) for 224 d of aging. This can be attributed to a slight increase in the mobility of the polymeric chains, which causes increase in the viscous loss and a horizontal shift towards right is observed in the peak of tan δ. The creation of free volumes and increased mobility also leads to a decrease in the stiffness as measured from the storage modulus plateau before the glass transition temperature [33]. But as no apparent reduction in Tg values is observed, it can also be hypothesized that decrease in the mechanical properties could be attributed to mechanical changes like decrease in the fiber/matrix interfacial adhesion as pointed in out Huang [50] and Karbhari [63],which occurs in synergy with the chemical changes inside the polymer.

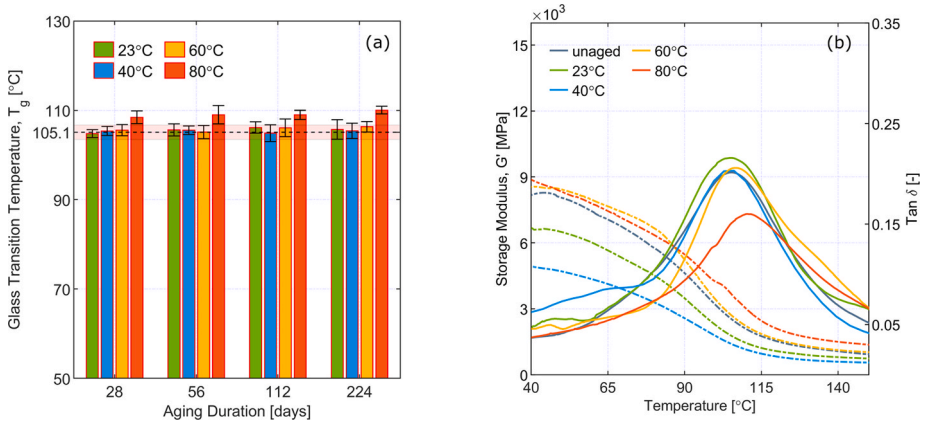

Fig. 15. (a) Variation of Tg values for thermally aged FWC coupons for 28, 56, 112 and 224 days and (b) representative curves of Tan δ and storage modulus values as function of aging temperature for 224 days of thermal exposure.

Fig. 15 (a) presents the changes in Tg values and (b) dynamic properties representative curves of storage modulus and damping factor (tan δ) of thermally aged FWC coupons after 224 d. For aging at temperatures of 23 °C, 40 °C and 60 °C, which are well below the Tg value of the unaged material, the changes observed are marginal when compared to the reference/unaged Tg value (105.1 ± 1.6 °C) and well within the standard deviation. An increase in the Tg values for aging at 80 °C was recorded even in the beginning of the aging period, which was also recorded for the case of hygrothermal aging.

For long-term aging, at low aging temperatures, the changes in Tg values are negligible where an apparent change of 0.5 °C, 0.3 °C, and 1.2 °C is calculated for aging at 23 °C, 40 °C and 60 °C after 224 d of aging. For aging at temperatures close to 0.75 Tg (80 °C), a substantial increment and time-temperature coupling of the Tg values was noted where an increment of 5 °C was recorded after a duration of 224 d at 80 °C. The viscoelastic changes are presented exemplary in Fig. 15 (b) where the peak of the damping factor reduces significantly, and a widening of the peak is also visible after 224 d of aging. This behavior can be attributed to thermally activated additional crosslinking, which leads to decreases in the polymeric chain mobility and hence a decrease in the viscous losses and an apparent increase in the stiffness values reflected by the storage modulus values. A similar observation has also been reported by Goertzen et al. [64]. As the aging temperature increases, the magnitude of the damping factor, decreases slightly and curve peaks shift towards the right-hand side of the chart, which signifies residual post-curing.

A similar strengthening and then degradation in properties from storage modulus (G') at room temperature is also observed in Fig. 16 for (a) hygrothermally and (b) thermal aged composites. Tables 11 and 12 tabulates the damping factor and storage moduli for both aging regimes. A higher degree of post-curing can be visible in coupons in hygrothermal environments. Comparing FWC response to thermal and hygrothermal aging, the results can be broadly divided into 2 main effect-categories viz: the effect of aging water and the effect of aging duration. When compared, it can be hypothesized that the presence of water increases the plasticization effect and causes high degree of crosslinking of the polymeric chain which results in an incremental shift in Tg values. Nonetheless, when the aging temperature approximates the reference Tg value, degradation and post-curing are competitively activated. The increased aging temperature activates molecular mobility and causes crosslinking which could also lead to an apparent increase in the recorded Tg values. The decrease in the mechanical properties, which is more prominent occurs much earlier in the case of hygrothermal aging, could be attributed to the mechanical degradation factors like fiber/matrix interfacial degradation or internal microstructure rearrangements, which could create sights for crack initiation and propagation under an applied load i.e. flexural.

3.5.2. *Color analysis and FTIR*

This sub-section presents the colour and FTIR analyses of the unaged and aged FWC coupons of the study. Fig. 17 presents the changes in the yellowing index of hygrothermally and thermally aged FWC coupons as a function of aging duration. As can be seen, FWC coupons exposed to hygrothermal and thermal aging, at same temperature and duration of

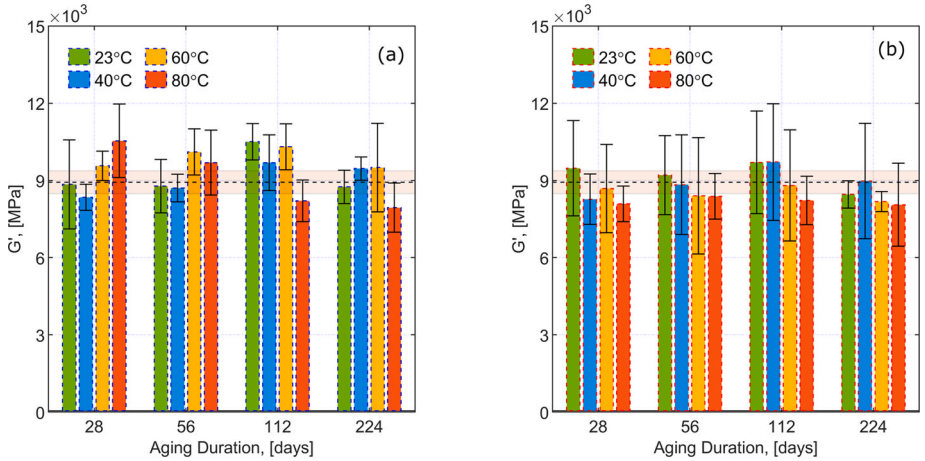

Fig. 16. Storage modulus (G') value at room temperature from DMA curves. (a) hygrothermal aging (b) thermal aging.

Table 11
Average Tg and corresponding y intercept of damping factor (tan δ) with standard deviation for hygrothermal aged FWC coupons.

Days	Room Temperature (23 °C)		40 °C		60 °C		80 °C	
	tan δ	Tg (°C).	tan δ	Tg (°C).	tan δ	Tg (°C).	tan δ	Tg (°C).
28	0.16 ± 0.02	104.7 ± 0.9	0.20 ± 0.02	105.3 ± 1.0	0.22 ± 0.03	105.5 ± 1.2	0.19 ± 0.03	108.4 ± 1.4
56	0.17 ± 0.04	105.6 ± 1.3	0.20 ± 0.01	105.5 ± 0.9	0.22 ± 0.03	105.1 ± 1.5	0.22 ± 0.03	109.1 ± 2.0
112	0.18 ± 0.04	106.1 ± 1.3	0.21 ± 0.04	104.8 ± 1.9	0.22 ± 0.04	106.1 ± 2.0	0.23 ± 0.03	109.1 ± 1.0
224	0.20 ± 0.03	105.6 ± 2.2	0.22 ± 0.03	105.4 ± 1.7	0.23 ± 0.03	106.3 ± 1.1	0.24 ± 0.02	110.1 ± 0.9

Table 12
Average Tg and corresponding y intercept of damping factor (tan δ) with standard deviation for thermal aged FWC coupons.

Days	Room Temperature (23 °C)		40 °C		60 °C		80 °C	
	tan δ	Tg (°C).	tan δ	Tg (°C).	tan δ	Tg (°C).	tan δ	Tg (°C).
28	0.23 ± 0.04	105.1 ± 3.1	0.24 ± 0.04	105.5 ± 1.9	0.20 ± 0.00	105.2 ± 1.2	0.21 ± 0.02	108.8 ± 1.7
56	0.21 ± 0.04	104.7 ± 2.0	0.22 ± 0.03	104.1 ± 1.2	0.24 ± 0.02	105.9 ± 0.6	0.22 ± 0.00	108.8 ± 0.2
112	0.23 ± 0.01	103.1 ± 2.4	0.24 ± 0.1	105.7 ± 2.0	0.21 ± 0.05	105.4 ± 2.1	0.20 ± 0.02	111.1 ± 0.2
224	0.24 ± 0.02	103.3 ± 1.1	0.20 ± 0.03	103.8 ± 0.9	0.20 ± 0.03	107.3 ± 0.9	0.19 ± 0.01	111.1 ± 1.4

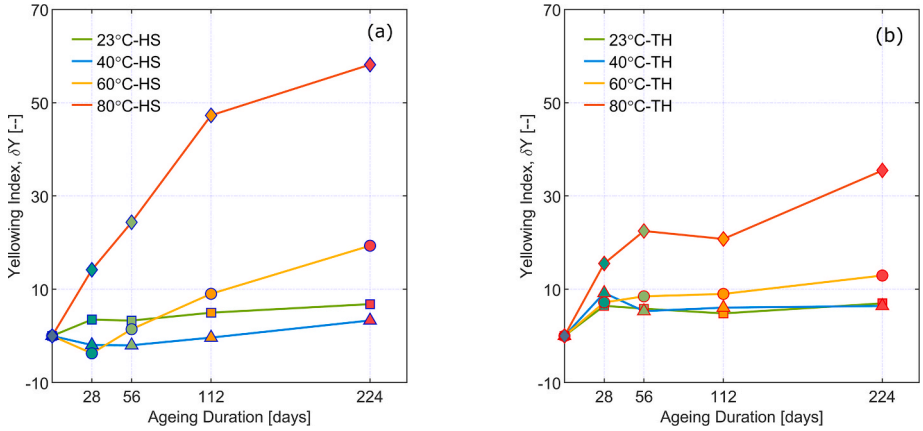

Fig. 17. Changes in the yellowing index of FWC coupons as a function of aging duration (a) hygrothermal (b) thermal environments.

aging, presented a different color loci after each aging interval. The color change was found to become darker when compared to the unaged reference coupon.

In the case of short-term aging (0–56 d), the yellowing due to hygrothermal aging at 23 °C is negligible. Interestingly, for aging at 40 °C and 60 °C, a reversal of yellowing is observed where the overall color change shifts towards the greener side as visible also in CIEXY colorspace plot presented in Fig. 18. Although, the reason behind this change is not fully understood, it can be hypothesized that an increase in the temperature may have led to increased water diffusion kinetics causing a lightning in color, but is not high enough for a chemical reaction to cause yellowing. A clear change in the yellowing index is visible for aging at 80 °C. For long term hygrothermal aging (56–224 d), the yellowing index increases fast in the beginning of aging, but then slows down towards the end of aging regime. No substantial yellowing was observed for coupons aged at T < 0.5 Tg (23 °C and 40 °C). Slight yellowing is observed at 60 °C at 20.1 points (pts). At 80 °C the browning is substantial (59 pts) and is nearly 4 times than that observed at lower aging temperatures.

In the case of short-term thermal aging (0–56 d), the yellowing of the structure did not exhibit a negative value and increases very slowly for aging temperature well below the Tg of the reference material. The degree of yellowing is very high at 80 °C and is nearly twice in magnitude when compared with that recorded for aging at lower temperatures. For long-term aging, the rate of yellowing slows down and even plateaus for aging at 23 °C and 40 °C. Increments are still visible for aging at 60 °C and 80 °C, where the change at 60 °C is much lower. For aging at 80 °C, the recorded yellowing is substantial (35 pts), and is nearly twice the scale when compared to that recorded for aging at lower temperatures. The color change loci after 224 d of aging at different temperatures is presented in Fig. 19.

The color changes are be attributed to thermo-oxidation of the carbonyl group and hydrolysis due to water ingress, leading to eventual chemical changes. The overall color change also becomes an area of interest to quantify changes in the outlook of the structure and can be tracked using the FTIR fingerprint of the material. FTIR spectral data is used to monitor potential changes of the chemical fingerprint of the studied FWC material and also contradict with the color and mechanical properties changes. No changes in the fiber reinforcement, related to morphology and chemical structure was assumed, hence only scrapes of the vinyl-ester resin from the top of the composite specimens were tested. The resin was scrapped from the surface and tested in ATR mode and the FTIR spectrum is presented in Fig. 20. As it is known, vinyl-ester monomer polymerizes through free radical polymerization [65] and may be susceptible to degradation through hydrolysis and oxidation in the presence of degradation agents like high temperature, water and their synergistic effects, which can be tracked in both the fingerprint and group frequency region of the FTIR curves.

The typical peaks visible in the spectra are the –OH peak between 3300 and 3400 cm^{-1}, –C═O stretching at 1722 cm^{-1}, styrene bending at 765 $cm^{-1,}$ and double –C═C at 827 cm^{-1}. Due to different absorption intensities, the extent of the oxidation and degradation can be determined by comparing the relative peak heights. To assess, the changes, FTIR results at the end of the aging duration of 224 d for both

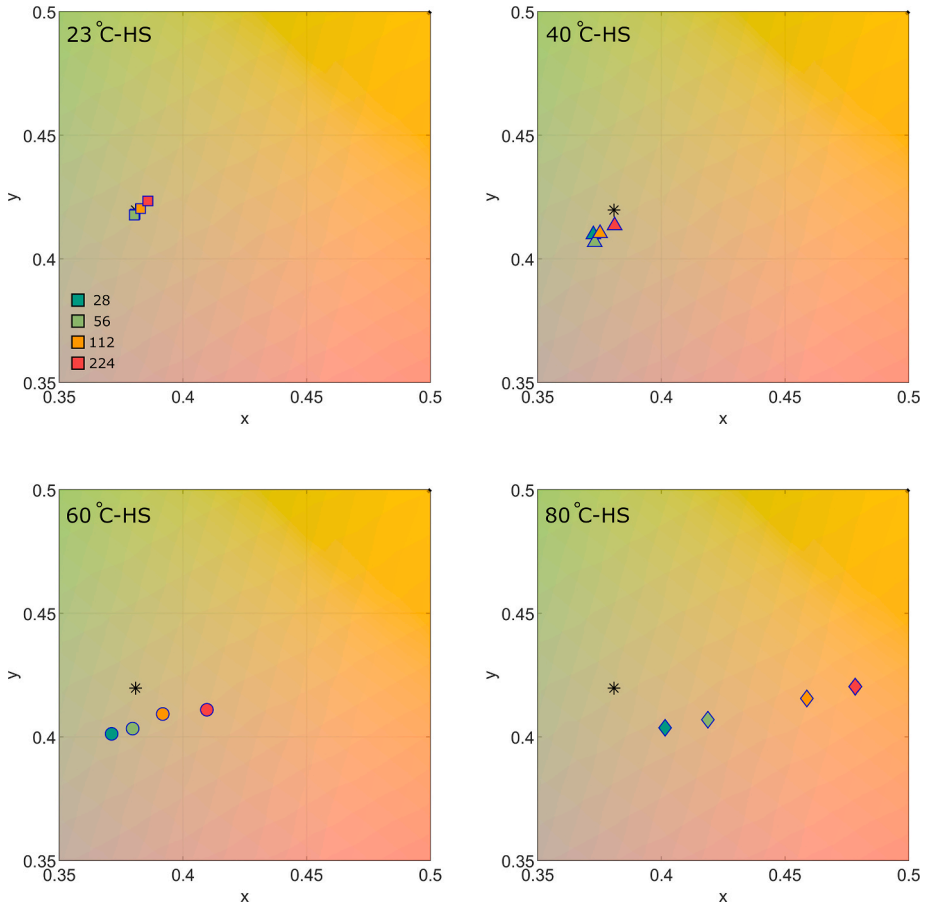

Fig. 18. Enlarged view of the CIEXYZ x,y colorspace for hygrothermally aged FWC coupons aged. The color coding in top left figure denotes the different duration of the aging.

hygrothermal and thermal environments are presented as an example.

Small changes in the infrared spectral were detected, consisting of:

1. A partial broadening and increase in the –C═O peak height and area observed as the temperature of the thermal aging increased from 23 °C to 80 °C after a duration of 224 d as presented in Fig. 21. A minimal increase in the –OH peak at 3034 cm^{-1} was also recorded which could be attributed to moisture uptaken.
2. A reduction in the –C═O carbonyl peak and hydroxyl (–OH) peak height as the aging temperature increases from 23 °C to 80 °C for the case of hygrothermal aging after 224 d of aging.

With respect to the FTIR spectra of the hygrothermally aged FWC coupons, it is a general trend that the intensity of the peak for the –C═O reduces as the aging temperature and duration increase. To compare the extent of degradation, the carbonyl index (measured as the ratio of the peak height at 1722 cm^{-1} and the peak at 1454 cm^{-1}) decreases. This in contrast to a slight increase in the carbonyl index after thermally aging FWCs coupons. While a decrease in the carbonyl index may be expected as a result of aging processes, this highlights that the carbonyl index alone is not a direct measure of degradation processes for these materials. It can be postulated that the chromophore content also increased for the thermally aged FWCs coupon, but not as highly as for the hygrothermally aged FWCs coupon. When comparing the hygrothermal and thermal aging environments, the chromophoric content is more pronounced in the case of hygrothermal aging and could lead to the creation of quinone. The quinone is a stronger chromophore due to a larger molar extinction coefficient that is likely to lead to a darker color compared to conjugated double bonds.

4. Conclusions

In summary, as part of a large research programme, this work presented findings of a comparison of the effects of accelerated hygrothermal and thermal aging on the mechanical and physico-chemical properties of a multilayered filament wound composite material (with a thermoplastic liner). The main findings can be summed up as follows:

1. The effect of hygrothermal aging caused more pronounced effect as compared to thermal aging, which can be attributed to the high sensitivity of vinylester matrix and fiber matrix interface towards moisture plasticization, hydrolytic leaching of interface and matrix material and temperature activated residual cross linking.
2. ILSS and flexure properties, both showed a non-monotonic behavior for aging at low temperatures, where-in an increase in properties was observed during short term aging, followed by a reduction phase and an eventual degradation where P(t) $<$ 100 %. A monotonic degradation was recorded at higher temperatures (80 °C), where chain mobility increases, causing rearrangements, bond breakage and eventual degradation.
3. The fractographic analysis suggests, the presence of pitted formation and fiber/matrix debonding, which could indicate a decrease in the interfacial strength for specimens aged under hygrothermal aging environment at higher temperature and longer duration of exposure.
4. The recorded increases in Tg values may be attributed to the increased crosslinking density with residual post-curing for both hygrothermal and thermal aging. This increase was more pronounced for the case of hygrothermal aging when compared to pure thermal aging. Degradation of fiber/matrix interface was caused by

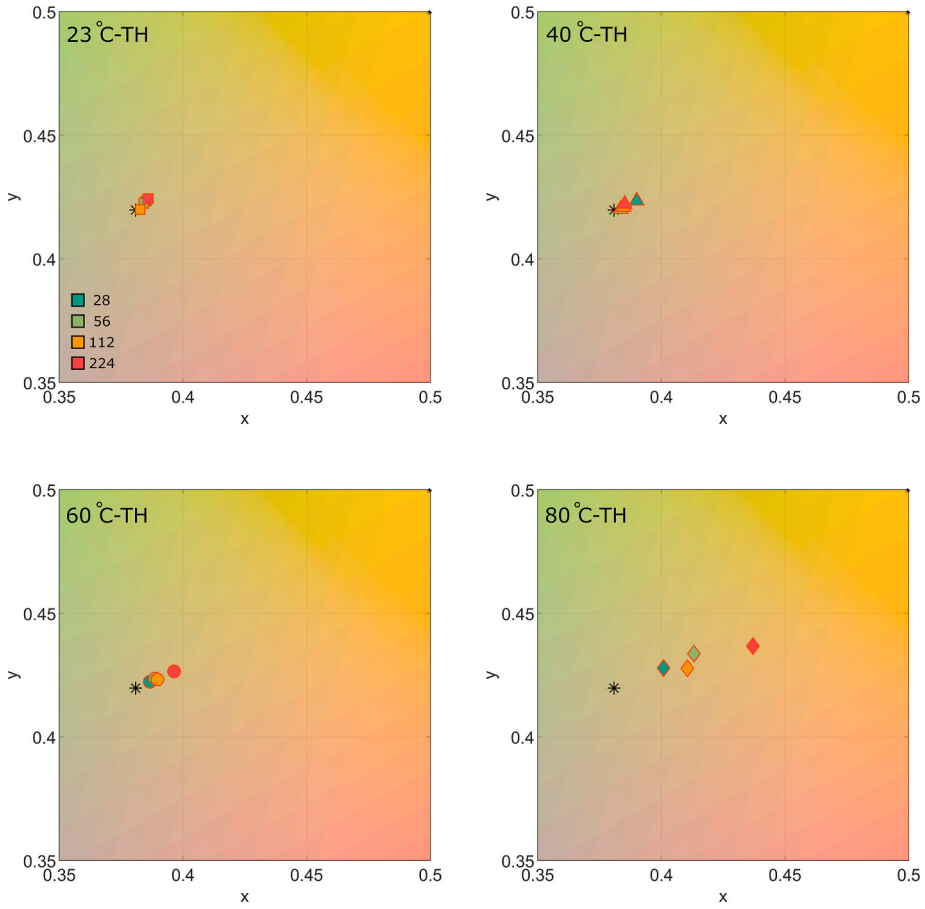

Fig. 19. Enlarged view of the CIEXYZ x,y colorspace for thermally aged FWC coupons. The color coding in top left figure denotes the different duration of the aging.

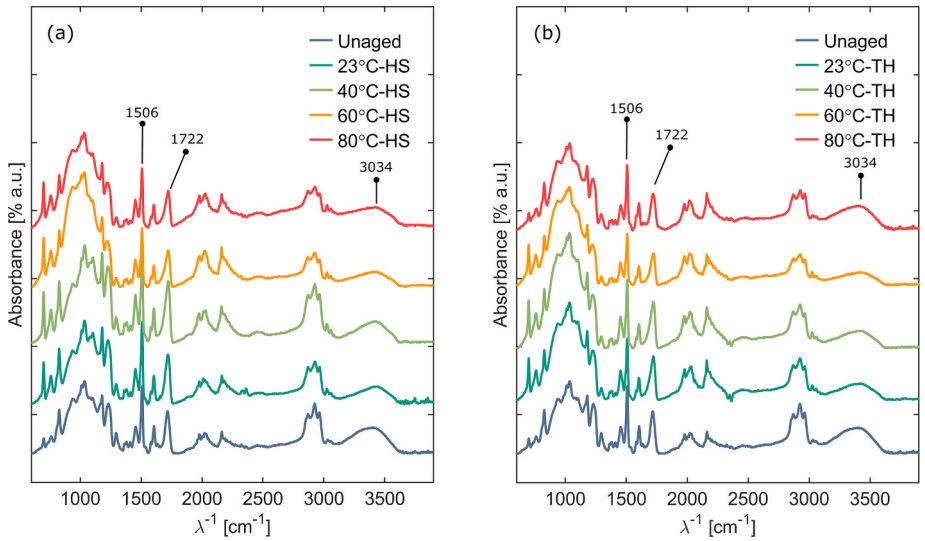

Fig. 20. ATR-FTIR spectra of (a) hygrothermally (b) thermal-aged FWC coupons for a duration of 224 days.

hygrothermal aging which was manifested as an increase in the damping factor whereas, a decrease in the damping factor was observed for the case of thermally aged coupons, signifying a decrease in chain mobility which could be attributed to post-curing.

5. A color change analysis coupled with FTIR showed the change of chemical formula, whereas a widening of –OH band, which is sign of hydrolytic attack on the vinylester, was also pinpointed. Carbonyl conversion was also noted, wherein a deepening yellow color was recorded for hygrothermal aging, attributed to decrease in ca. 1720 cm^{-1} peak as a result of carbonyl conversion.

In summary, this study provides a deep insight on the effects of

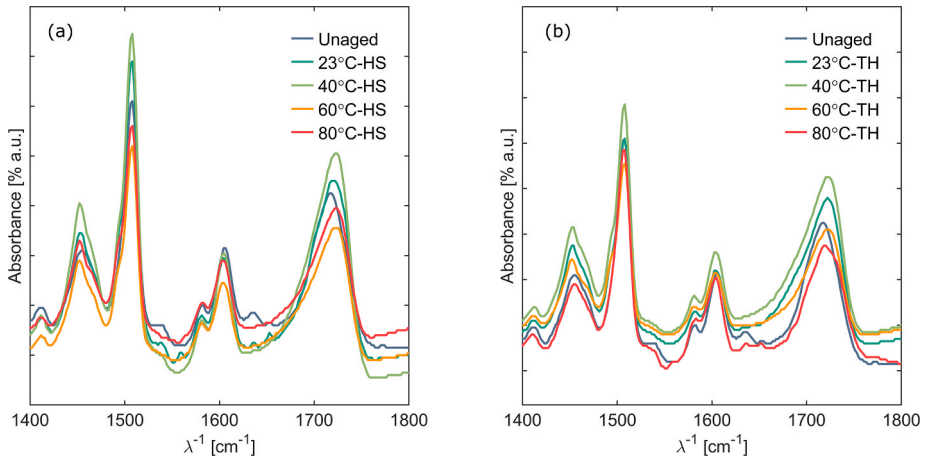

Fig. 21. Inset FTIR curves with carbonyl peaks (1720 cm^{-1}) (a) hygrothermal static (H.S.) (b) thermal aging (T.H.).

accelerated hygrothermal and thermal aging on the mechanical and physicochemical properties of a multilayered (with liner) filament wound composite. Given the complexity of the material itself, more work is needed, in order to enhance the understanding of background effects, that are reflected as mechanical property changes. Since filament winding is gaining increasing attention by the industry, given the versatility and automation potential of the method, in the absence of design guidelines and lifetime prediction tools, the results of this work, can function as the foundation to create novel prediction models for lifetime prediction of filament wound composite structures and hence provide essential recommendations and definitions to account for material degradation when designing GFRP structures made of filament winding.

CRediT authorship contribution statement

Chaman Srivastava: Conceptualization, Data curation, Formal analysis, Investigation, Methodology, Software, Visualization, Writing – original draft. **Ben Alcock:** Supervision, Validation, Writing – review & editing. **Are Strandlie:** Supervision, Writing – review & editing. **Sotirios A. Grammatikos:** Conceptualization, Methodology, Project administration, Supervision, Validation, Writing – review & editing.

Declaration of competing interest

The authors declare that they have no known competing financial interests or personal relationships that could have appeared to influence the work reported in this paper.

Data availability

The authors do not have permission to share data.

Acknowledgement

The work reported in this paper is based on activities within the center for research-based innovation SFI Manufacturing in Norway and is partially funded by the Research Council of Norway under contract number 237900. The author also acknowledges the support from the projects PREDICT (Ref: 297069) and LIFETIME (Ref: 309943), funded by the Research Council of Norway.

References

[1] T.A. Sebaey, Design of oil and gas composite pipes for energy production, Energy Proc. 162 (2019) 146–155.
[2] A. Gibson, et al., Non-metallic pipe systems for use in oil and gas, Plast., Rubber Compos. 40 (10) (2011) 465–480.
[3] A.O. Olorunnisola, Potentials of Wood, bamboo and natural fiber-reinforced composite products as substitute materials for fabricating affordable agricultural equipment and processing machines in Africa, in: Technology in Agriculture, IntechOpen, 2021.
[4] H. Energy, Composite insulators, Available from: https://www.hitachienergy.com/products-and-solutions/transformer-insulation-and-components/composite-insulators, 2022.
[5] P. Mertiny, F. Ellyin, Influence of the filament winding tension on physical and mechanical properties of reinforced composites, Compos. Appl. Sci. Manuf. 33 (12) (2002) 1615–1622.
[6] C. Srivastava, et al., Three-dimensional analysis of porosity in as-manufactured glass fiber/vinyl ester filament winded composites using X-ray micro-computed tomography, Appl. Compos. Mater. (2023) 1–30.
[7] V. Karbhari, et al., Durability gap analysis for fiber-reinforced polymer composites in civil infrastructure, J. Compos. Construct. 7 (3) (2003) 238–247.
[8] R. Rafiee, On the mechanical performance of glass-fiber-reinforced thermosetting-resin pipes: a review, Compos. Struct. 143 (2016) 151–164.
[9] S.-N. Nguyen, et al., A coupled hygrothermo-mechanical viscoelastic analysis of multilayered composite plates for long-term creep behaviors, Compos. Struct. 242 (2020) 112030.
[10] L.C. Bank, et al., A model specification for FRP composites for civil engineering structures, Construct. Build. Mater. 17 (6–7) (2003) 405–437.
[11] P. Purnell, et al., Service life modelling of fiber composites: a unified approach, Compos. Sci. Technol. 68 (15–16) (2008) 3330–3336.
[12] K. Pickering, M. Beg, Quality and durability of recycled composite materials, in: Management, Recycling and Reuse of Waste Composites, Elsevier, 2010, pp. 303–327.
[13] J.T. Mottram, et al., Design of fiber-polymer composite structures–European Technical Specification: combined stresses, in: 20th European Conference on Composite Materials: Composites Meet Sustainability, EPFL Lausanne, Composite Construction Laboratory, 2022.
[14] E. Barjasteh, et al., Thermal aging of fiberglass/carbon-fiber hybrid composites, Compos. Appl. Sci. Manuf. 40 (12) (2009) 2038–2045.
[15] S.A. Grammatikos, et al., On the response to hygrothermal aging of pultruded FRPs used in the civil engineering sector, Mater. Des. 96 (2016) 283–295.
[16] A.R. Berens, H.B. Hopfenberg, Diffusion and relaxation in glassy polymer powders: 2. Separation of diffusion and relaxation parameters, Polymer 19 (5) (1978) 489–496.
[17] T. Morii, et al., Weight changes of a randomly orientated GRP panel in hot water, Compos. Sci. Technol. 49 (3) (1993) 209–216.
[18] J. Zhou, J.P. Lucas, Hygrothermal effects of epoxy resin. Part II: variations of glass transition temperature, Polymer 40 (20) (1999) 5513–5522.
[19] N. Hancox, Thermal effects on polymer matrix composites: Part 2. Thermal degradation, Mater. Des. 19 (3) (1998) 93–97.
[20] T. Tsotsis, Thermo-oxidative ageing of composite materials, in: Ageing of Composites, Elsevier, 2008, pp. 130–159.
[21] J. Fan, X. Hu, C.Y. Yue, Thermal degradation study of interpenetrating polymer network based on modified bismaleimide resin and cyanate ester, Polym. Int. 52 (1) (2003) 15–22.
[22] K.V. Pochiraju, Modeling thermo-oxidative aging and degradation of composites, in: Long-term Durability of Polymeric Matrix Composites, Springer, 2012, pp. 383–425.
[23] J. Decelle, N. Huet, V. Bellenger, Oxidation induced shrinkage for thermally aged epoxy networks, Polym. Degrad. Stabil. 81 (2) (2003) 239–248.
[24] O. Starkova, et al., Water transport in epoxy/MWCNT composites, Eur. Polym. J. 49 (8) (2013) 2138–2148.
[25] Y. Joliff, et al., Study of the moisture/stress effects on glass fiber/epoxy composite and the impact of the interphase area, Compos. Struct. 108 (2014) 876–885.

[26] K. Liao, C. Schultheisz, D.L. Hunston, Effects of environmental aging on the properties of pultruded GFRP, Compos. B Eng. 30 (5) (1999) 485–493.
[27] T. Skourlis, R. McCullough, The effect of temperature on the behavior of the interphase in polymeric composites, Compos. Sci. Technol. 49 (4) (1993) 363–368.
[28] K. Derrien, P. Gilormini, The effect of moisture-induced swelling on the absorption capacity of transversely isotropic elastic polymer–matrix composites, Int. J. Solid Struct. 46 (6) (2009) 1547–1553.
[29] X. Buch, M. Shanahan, Thermal and thermo-oxidative ageing of an epoxy adhesive, Polym. Degrad. Stabil. 68 (3) (2000) 403–411.
[30] A.E. Krauklis, A.T. Echtermeyer, Mechanism of yellowing: carbonyl formation during hygrothermal aging in a common amine epoxy, Polymers 10 (9) (2018) 1017.
[31] I. Ksouri, O. De Almeida, N. Haddar, Long term ageing of polyamide 6 and polyamide 6 reinforced with 30% of glass fibers: physicochemical, mechanical and morphological characterization, J. Polym. Res. 24 (2017) 1–12.
[32] N. Allen, et al., Photo-oxidative stability of electron beam and U.V. cured acrylated epoxy and urethane acrylate resin films, Polym. Degrad. Stabil. 19 (2) (1987) 147–160.
[33] S. Cabral-Fonseca, et al., Artificial accelerated ageing of GFRP pultruded profiles made of polyester and vinylester resins: characterisation of physical–chemical and mechanical damage, Strain 48 (2) (2012) 162–173.
[34] D. Rosu, L. Rosu, C.N. Cascaval, Effect of ultraviolet radiation on vinyl ester network based on bisphenol A, J. Photochem. Photobiol. Chem. 194 (2–3) (2008) 275–282.
[35] S.C. Das, et al., Effect of accelerated weathering on the performance of natural fiber reinforced recyclable polymer composites and comparison with conventional composites, Composites Part C: Open Access (2023) 100378.
[36] S.C. Das, et al., On the response to hygrothermal ageing of fully recyclable flax and glass fiber reinforced polymer composites, Materials 16 (17) (2023) 5848.
[37] S. Grammatikos, et al., Moisture uptake characteristics of a pultruded fiber reinforced polymer flat sheet subjected to hot/wet aging, Polym. Degrad. Stabil. 121 (2015) 407–419.
[38] D/DM-20, A., Standard Test Method for Moisture Absorption Properties and Equilibrium Conditioning of Polymer Matrix Composite Materials, ASTM International West, Conshohocken, PA, 2020.
[39] D. Valentin, F. Paray, B. Guetta, The hygrothermal behaviour of glass fiber reinforced Pa66 composites: a study of the effect of water absorption on their mechanical properties, J. Mater. Sci. 22 (1) (1987) 46–56.
[40] D. Astm, 2344 Standard Test Method for Short-Beam Strength of Polymer Matrix Composite Materials and Their Laminates, ASTM, West Conshohocken, PA, USA, 2016.
[41] L. Wu, et al., Short-term effects of sea water on E-glass/vinylester composites, J. Appl. Polym. Sci. 84 (14) (2002) 2760–2767.
[42] P. Green, L. MacDonald, Colour Engineering: Achieving Device Independent Colour, John Wiley & Sons, 2011.
[43] E. Astm, E313-05 Standard practice for calculating yellowness and whiteness indices from instrumentally measured color coordinates, Paint-Tests Chem., Phys., Optical Prop. (2005).
[44] L.-R. Bao, A.F. Yee, C.Y.-C. Lee, Moisture absorption and hygrothermal aging in a bismaleimide resin, polymer 42 (17) (2001) 7327–7333.
[45] X. Jiang, H. Kolstein, F.S. Bijlaard, Moisture diffusion in glass–fiber-reinforced polymer composite bridge under hot/wet environment, Compos. B Eng. 45 (1) (2013) 407–416.
[46] J. Sousa, et al., Hygrothermal ageing of pultruded GFRP profiles: comparative study of unsaturated polyester and vinyl ester resin matrices, Compos. Appl. Sci. Manuf. 140 (2021) 106193.
[47] Y. Yu, et al., Hygrothermal aging on pultruded carbon fiber/vinyl ester resin composite for sucker rod application, J. Reinforc. Plast. Compos. 25 (2) (2006) 149–160.
[48] H. Xin, et al., Moisture diffusion and hygrothermal aging of pultruded glass fiber reinforced polymer laminates in bridge application, Compos. B Eng. 100 (2016) 197–207.
[49] D. Lau, et al., Long term performance and fire safety aspect of FRP composites used in building structures, Construct. Build. Mater. 126 (2016) 573–585.
[50] H. Gu, Dynamic mechanical analysis of the seawater treated glass/polyester composites, Mater. Des. 30 (7) (2009) 2774–2777.
[51] G. Odegard, A. Bandyopadhyay, Physical aging of epoxy polymers and their composites, J. Polym. Sci. B Polym. Phys. 49 (24) (2011) 1695–1716.
[52] V. Karbhari, E-glass/vinylester composites in aqueous environments: effects on short-beam shear strength, J. Compos. Construct. 8 (2) (2004) 148–156.
[53] L. Gautier, B. Mortaigne, V. Bellenger, Interface damage study of hydrothermally aged glass-fiber-reinforced polyester composites, Compos. Sci. Technol. 59 (16) (1999) 2329–2337.
[54] L. Salmon, et al., Hydrolytic degradation of model networks simulating the interfacial layers in silanecoupled epoxy/glass composites, Compos. Sci. Technol. 57 (8) (1997) 1119–1127.
[55] S. Marouani, L. Curtil, P. Hamelin, Ageing of carbon/epoxy and carbon/vinylester composites used in the reinforcement and/or the repair of civil engineering structures, Compos. B Eng. 43 (4) (2012) 2020–2030.
[56] J. Gong, et al., A numerical study of thermal degradation of polymers: surface and in-depth absorption, Appl. Therm. Eng. 106 (2016) 1366–1379.
[57] C. Srivastava, et al., A comparative study on the effect of hot/wet and hot/dry aging environments on the degradation of filament winded composites, in: Proceedings of the 20th European Conference on Composite Materials-Composites Meet Sustainability, vols. 1–6, EPFL Lausanne, Composite Construction Laboratory Switzerland, 2022.
[58] K. Verghese, et al., Influence of matrix chemistry on the short term, hydrothermal aging of vinyl ester matrix and composites under both isothermal and thermal spiking conditions, J. Compos. Mater. 33 (20) (1999) 1918–1938.
[59] W. Chu, V.M. Karbhari, Effect of water sorption on performance of pultruded E-glass/vinylester composites, J. Mater. Civ. Eng. 17 (1) (2005) 63–71.
[60] L.C.M. Barbosa, D.B. Bortoluzzi, A.C. Ancelotti Jr., Analysis of fracture toughness in mode II and fractographic study of composites based on Elium® 150 thermoplastic matrix, Compos. B Eng. 175 (2019) 107082.
[61] M.A. Meyers, K.K. Chawla, Mechanical Behavior of Materials, Cambridge university press, 2008.
[62] E. Greenhalgh, Failure Analysis and Fractography of Polymer Composites, Elsevier, 2009.
[63] V.M. Karbhari, Q. Wang, Multi-frequency dynamic mechanical thermal analysis of moisture uptake in E-glass/vinylester composites, Compos. B Eng. 35 (4) (2004) 299–304.
[64] W.K. Goertzen, M. Kessler, Dynamic mechanical analysis of carbon/epoxy composites for structural pipeline repair, Compos. B Eng. 38 (1) (2007) 1–9.
[65] C. Alia, et al., Characterization of the chemical structure of vinyl ester resin in a climate chamber under different conditions of degradation, Polym. Degrad. Stabil. 153 (2018) 88–99.